Journal of Engineering Technology and Applied Sciences, 2025 *e-ISSN:* 2548-0391
Received 22 October 2024, Accepted 11 February 2025 *Vol. 10, No. 1, 1-19*
Published online 29 April 2025, Research Article *doi: 10.30931/jetas.1571579*

Citation: Tezgel, M.B., Karaarslan, A., "Hybrid PSM-PWM Combined Modulation Applied to Bidırectional Dual Active Bridge CLLC Resonant Converter". Journal of Engineering Technology and Applied Sciences 10 (1) 2025 : 1-19.

HYBRID PSM-PWM COMBINED MODULATION APPLIED TO BIDIRECTIONAL DUAL ACTIVE BRIDGE CLLC RESONANT CONVERTER

Muhammet Beşer Tezgel[a*], Ahmet Karaarslan[a]

[a]Department of Electrical & Electronics Engineering, Institute of Science, Ankara Yıldırım Beyazıt University, Ankara, Turkey*
*mbtezgel@outlook.com (*corresponding author), akaraarslan@aybu.edu.tr, akaraarslan@gmail.com*

Abstract

This study investigates the application of a combined modulation approach, integrating both phase shift modulation (PSM) and pulse width modulation (PWM), in driving a bidirectional Capacitor-Inductor-Inductor-Capacitor (CLLC) dual active bridge (DAB) resonant converter. Unlike conventional hybrid switching techniques, wherein the system toggles between PWM and PSM signals, this proposed method introduces a unified modulation signal for the switching process. The dynamic control of two modulation parameters, namely duty ratio and phase shift angle, plays a pivotal role in shaping the switching sequence. Adopting this innovative methodology yields notable advantages, such as reducing output ripple and preventing resonant effects on the desired output waveform. The implementation of this system is carried out using the MATLAB/SIMULINK program, facilitating comprehensive validation across various operational modes such as buck, boost, and unity operations.

Keywords: PI control, combined modulation, phase shift modulation, pulse width modulation, CLLC resonant converter

1. Introduction

Power converters have a significant role in a wide application area, and they ought to provide more efficiency and flexibility day by day [1, 2]. Electric vehicle (EV) charging systems widely use DC-DC converters [3]. Bidirectional resonant converters are generally preferred due to their numerous advantages [4]. One of them is the inherent zero-voltage switching (ZVS) and zero-current switching (ZCS) capability at the primary and secondary side of the converter, respectively, which verifies its high efficiency characteristics [5]. The LLC converter's unidirectional operation prompts the introduction of a bidirectional full bridge CLLC resonant converter. Additionally, CLLC resonant converter eliminates the requirement of snubber

circuits [6]. The ability to provide exactly the same power conversion and efficiency for both forward and reverse energy flow [7], especially, makes it suitable for EV charge applications since EVs can be both energy storage or consumption component of grids. Moreover, as DC Transformers (DCXs), CLLC resonant converters are an attractive choice because of their high efficiency characteristics [8]. There are many studies with DCXs used in various applications like energy storing applications, vehicle-to-grid (V2G) applications, or AC/DC microgrid applications, as discussed in [9-11].

Power converters are able to serve higher power factor, lower harmonics, and rapid responses as control strategies are developed and optimized [12]. DAB topology is commonly used together with CLLC topologies, and, since soft switching is challenging for the DAB converter, there must be a complex control structure for modulation [13].

Each control method focuses on handling the desired yield value of a system. Controllers provide preset values at the output terminal for power converters. The study [14] confirms a control principle that relies on a variable phase difference. Besides, an analysis of multiphase shift control is evaluated in [15]. There is a discussion and compilation of modulation strategies on [16], in which pulse frequency modulation (PFM) is mentioned as the one that is most commonly used. However, a wide range of frequency variations cause complications in the design and optimization of magnetic components, driver circuits, and EMI filters [16, 17]. Hybrid modulation techniques are developed to expand the converter's efficient range. A more stable output voltage claimed by many researchers proposed a combined usage of other control methods with PFM [18].

Some fixed frequency control techniques like PSM and asymmetrical pulse width modulation (APWM) are mentioned in [17]. However, all of these fixed frequency control techniques, including PSM and APWM, experience a loss of ZVS for a wide input voltage range when operating under light load according to [17]. The paper [19] presents a novel APWM control strategy to overcome this restriction. This method regulates the asymmetric gate signals at a resonant frequency for both upper and lower switches. There is another modulation strategy proposed in [20]. The study says that a PFM+PSM hybrid control strategy helps to raise efficiency and power density by reducing the range of switching frequencies. In short, there are considerable numbers of articles that investigate different types of single or hybrid modulation techniques. Some of the techniques mentioned in [21-24] include resonant frequency modulation (RFM), PFM+PWM hybrid modulation, and PSM+PFM hybrid modulation. Similar control techniques can be used for different power topologies, as [25] proposes a hybrid intelligent controller for a PV system.

In addition to different ways of controlling, CLLC converters have synchronous rectification, which gets rid of the voltage drop caused by the body diodes of the rectifying side switches. Studies [26–28] show some synchronous rectification methods and processes.

This paper is an extended work that describes the design and implementation of combined control techniques of PWM and PSM using a bidirectional DAB CLLC resonant converter with Continues Conduction Mode (CCM) operated at 11 kW. The method might be applied to various power converter topologies, on the other hand, the motivation behind this study is there is not any past study in literature that applies instant PWM&PSM combined modulation to a DAB CLLC resonant converter. In general, the paper is organized as follows: Section 2 clarifies the operation mode of the bi-directional CLLC-resonant DAB converter in CCM. Section 3 delves into the proposed control method for the converter and pinpoints its parameters.

Simulation results validate the operation of the bi-directional CLLC-resonant DC-DC converter in Section 4. Section 5 summarizes the main findings in this study.

2. Circuit description and operation

In power electronics, the best choice for the application must be chosen. To explain more, power electronic circuits are designed to achieve the desired result with the available maximum efficiency, lowest cost, and smallest size. CLLC resonant converters are very popular as DCX, so they are widely used in DC power conversion processes.

DAB CLLC resonant converter consists of eight switches, resonant tank components, a capacitor and an inductor, and a transformer. As shown in Fig. 1, this converter has a symmetrical structure, which allows bidirectional energy flow operation.

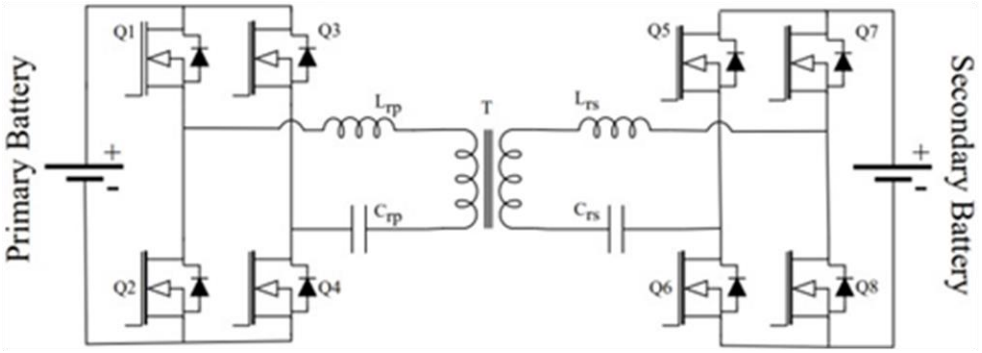

Figure 1. Bidirectional DAB CLLC resonant converter topology

Moreover, the switches on the rectifying side can also satisfy synchronous rectification (SR). SR prevents the losses of the body diodes by eliminating forward voltage drops. Next, Table 1 provides the circuit components, specifications, their values and units.

Table 1. Converter specifications.

Notation	Value	Unit
Primary battery	700-800	V
Secondary battery	550-800	V
L_{rp}	36	µH
L_{rs}	22	µH
L_m	160	µH
C_{rp}	132	nF
C_{rs}	216	nF

In this topology, a varying duty ratio switching signal drives Q1, and an identical one with a varying phase shift angle drives Q3, while the lower switches, Q2 and Q4, operate complementary to the upper ones, respectively.

A sense loop finds the resonant current on the input side and then creates switching signals that stop the diodes on the rectifier side from dropping their forward voltage. This makes synchronous rectification possible. By simultaneously adjusting these two parameters, duty

ratio and phase shift angle, the converter can be operated in buck, boost, and unity mode. The related equation between the input and output terminal voltages at steady state is formulated as given in Eq. (1).

$$V_p = G_f * \frac{1}{n} * V_s \tag{1}$$

where V_p is primary and V_s is secondary side terminal voltages, G_f is the forward resonant tank gain and n is transformer ratio.

Vice versa, relation between two sides of the system during reverse energy transmission is given by the Eq. (2).

$$V_s = G_r * n * V_p \tag{2}$$

where G_r is the reverse resonant tank gain. Since the switching frequency and transformer ratio remain fixed, the equations encompass all buck, boost, and unity operations. Phase shifting and pulse width adjustment hold the required conversion. Fig. 2 illustrates two alternating cycles in both forward and reverse transmission, while Section 3 discusses the system's more detailed working principle, control strategies, and proposed modulation.

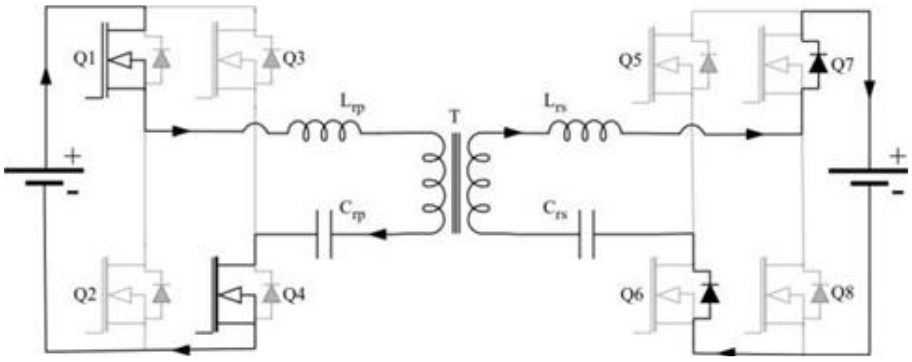

Figure 2.a Forward non-shifted leg operation

In forward energy transmission, primary DAB switches employed to inverting process. Fig. 2.a, shows the current flow path while non-shifted pulse switching the switch Q1. At the same time, Q4 is also in conduction mode.

With a phase shift angle of ϕ, switches Q2 and Q3 become in conductive mode as illustrated in Fig. 2.b, thus, second half of conducting period has been completed by current flow on implied pathway.

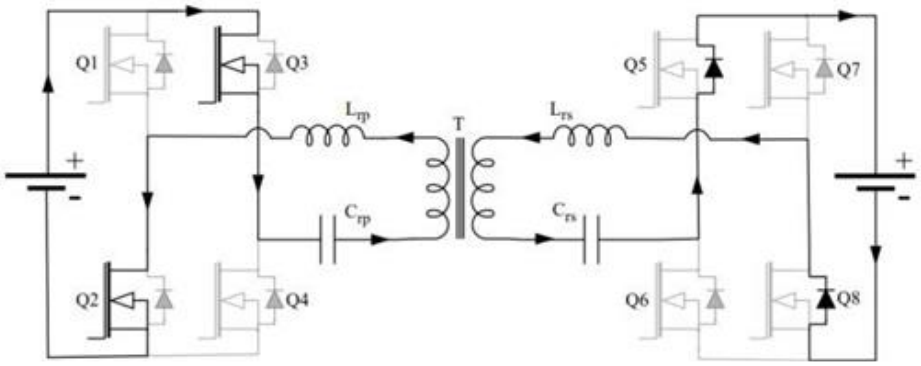

Figure 2.b Forward shifted leg operation

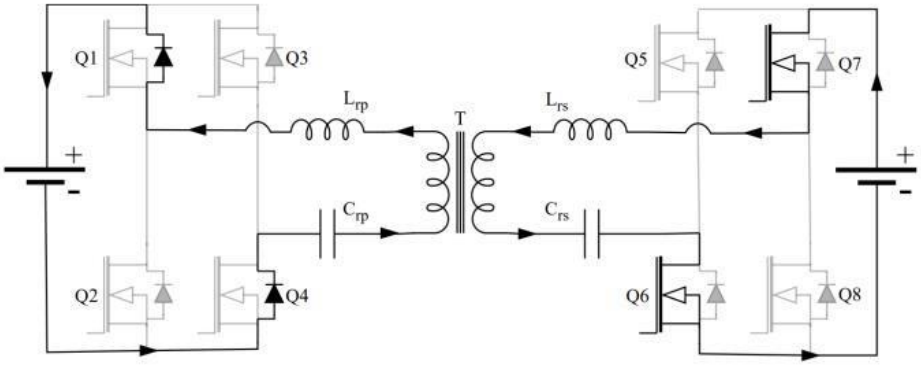

Figure 2.c Reverse non-shifted leg operation

For the reverse mode operation, Fig. 2.c reveals the non-shifted switching sequence of secondary DAB, where current flows through Q7 at upper and Q6 at bottom.

Finally, Fig. 2.d illustrates the reverse shifted switching operation of the converter. At this time, switches Q5 and Q8 are in conduction.

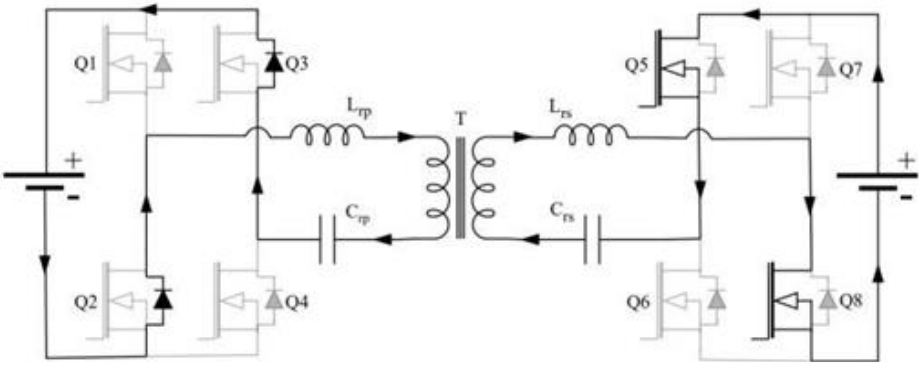

Figure 2.d Reverse shifted leg operation

3. Control and modulation strategies

Control systems are designed to stabilize the output of the plants under varying input voltage, load, or environmental conditions. PI controller is one of the most the most common control

method preferences in power electronics applications. The output of the controller is a driving signal, which could be generated in several modulation types.

This paper mentions some modulation types briefly and investigates a combined PWM&PSM modulation that adjusts pulse width and phase shift angle instantly. There are three different fixed frequency modulation methods that are compared in [29]. A PSM+PFM hybrid control strategy is focused [23, 24] to handle the challenges of some disadvantages of the CLLC resonant converter. Furthermore, another study [30] asserts that a PWM+PFM hybrid modulation strategy leads to a higher power efficiency. These types of research aim to improve the efficiency of the system while minimizing the size of the circuit. Furthermore, they generally are presenting new methods to eliminate systems' boundaries or widen them up.

Apart from common hybrid techniques, this paper presents a combined modulation method. Unlike switching between modulation types, each modulation affects the switching signal simultaneously. Fig. 3 depicts a block diagram of the system operating in the reversal CC mode. Basically, there are two independent control loops that track current or voltage (depending on CC or CV charge) and supply power at the output terminal. Two separate PI loops synchronize to determine the modulation parameters, while a pulse generator carries out the remaining tasks. Section 4 will present a detailed MATLAB simulation study, revealing voltage, current, and switching signal waveforms, among other ones.

The gain of the system depends on several parameters; they are resonant components, resonant frequency, switching frequency, Q factor, and implicitly load resistor. From fundamental harmonic analysis (FHA), as considered in Eq. (1), forward gain can be calculated by considering following equations: Eq. (3), Eq. (4), Eq. (5), Eq. (6) and Eq. (7).

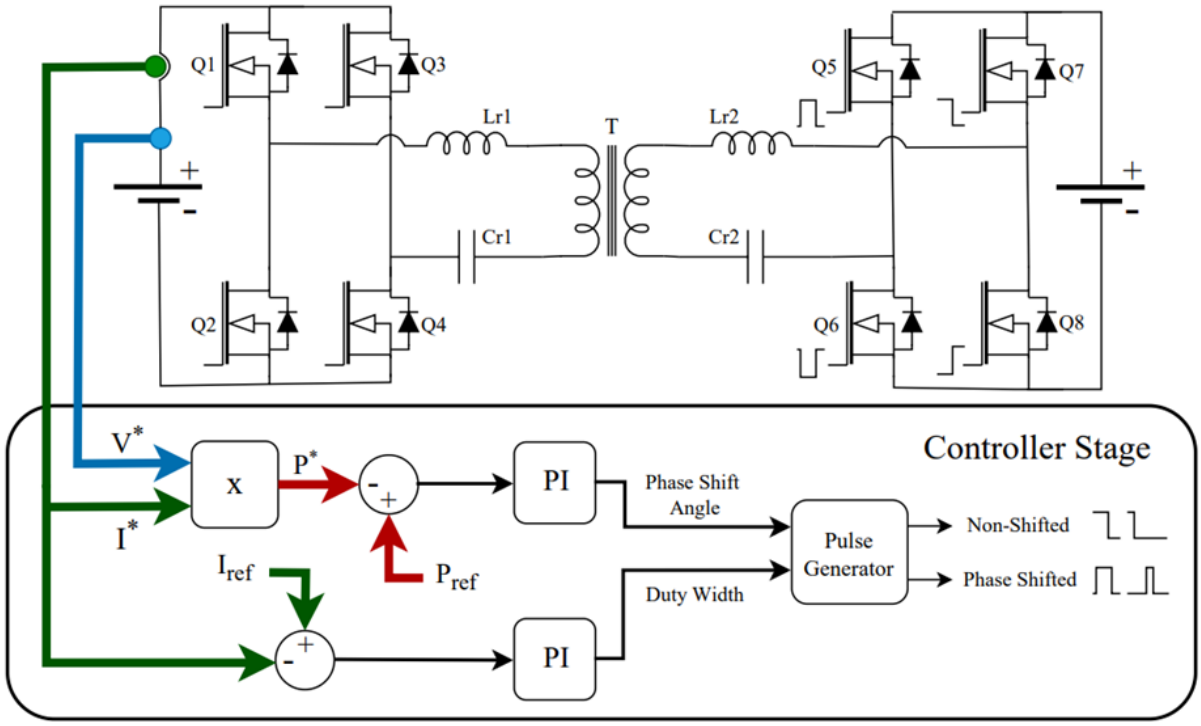

Figure 3. Block diagram of the general control process

$$G_f = \frac{1}{\sqrt{A^2 + B^2}} \tag{3}$$

where

$$A = \frac{1}{h} + 1 - \frac{1}{h * \omega_n^2} \tag{4}$$

and

$$B = Q_f * \left(\frac{1}{\omega_n} - \omega_n\right) + \frac{Q_f*(1+h)}{g*h*\omega_n} - \frac{Q_f}{g*h*\omega_n^3} \tag{5}$$

where h is the ratio of magnetizing inductance to primary resonant inductance, g is the ratio of the secondary capacitance to the primary capacitance and ω_n is the ratio of switching frequency to resonant frequency, whilst

$$Q_f = \frac{\sqrt{\frac{L_{S1}}{C_{S1}}}}{R_{eq}} \tag{6}$$

where

$$R_{eq} = \frac{8*n^2}{\pi^2} * R_{load} \tag{7}$$

The system has a resonant frequency of 73 kHz, and the switching frequency is 25 kHz. According to equations above, gain curve of the forward operating CLLC resonant tank up to 250 kHz with different Q values could be observed on Fig. 4. Additionally, Fig. 5 shows a zoomed view to gain curve at switching frequency.

Without any adjustment on phase shift angle and pulse width, Eq. (1) reveals the relation between input and output voltages. Besides, required voltage/current and power regulations are accomplished by two control loops.

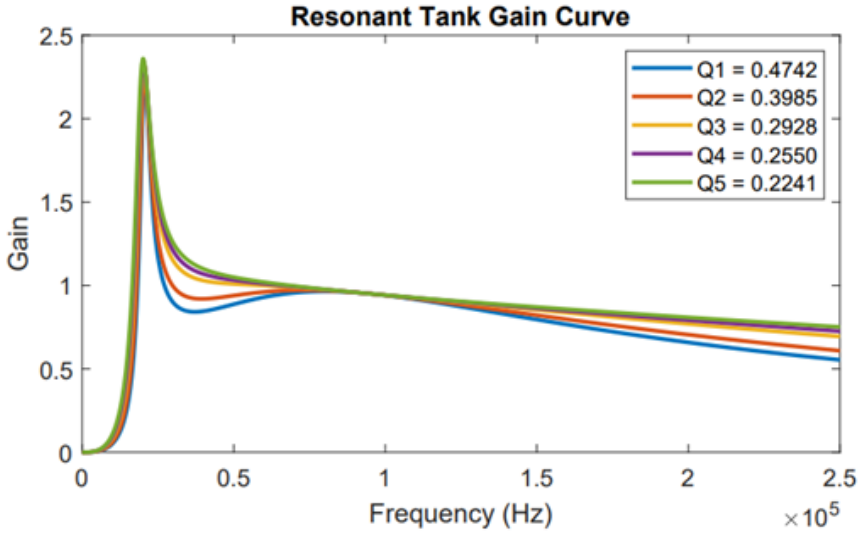

Figure 4. Resonant tank forward gain curve with related Q values

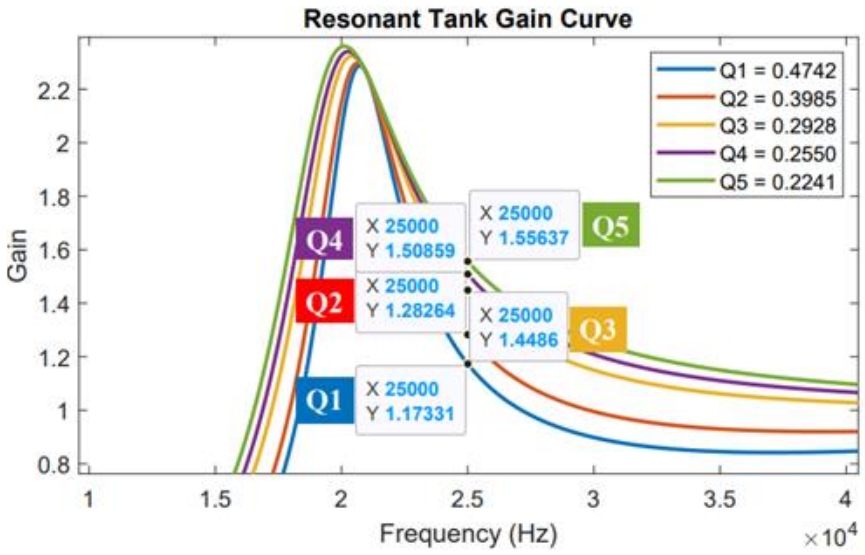

Figure 5. Resonant tank forward gains at switching frequency

4. Simulation studies and discussion

The section above concludes with an explanation of the open-loop control principle. When it comes to closed control loops, it is crucial to continuously track the desired system parameters. In Fig. 6, a flowchart-based process implements the presented modulation strategy. Following the steps outlined in the chart, the system continuously monitors the state of charge (SOC) status of the batteries, as well as any voltages or currents flowing through the batteries and the power supply at the output side. As anticipated, the system transfers energy from the battery with a higher state of charge (SOC) to the one with a lower SOC until both batteries reach the same SOC level. Next, the controller determines energy flow direction and operation mode. Given that the CLLC tank exhibits a gain greater than 1 in both forward and reverse operations, it appears to be operating in the boost mode.

PSM and PWM are the key points for the unity and buck mode operations. To understand and have a closer look at the system, a MATLAB/Simulink simulation was performed.

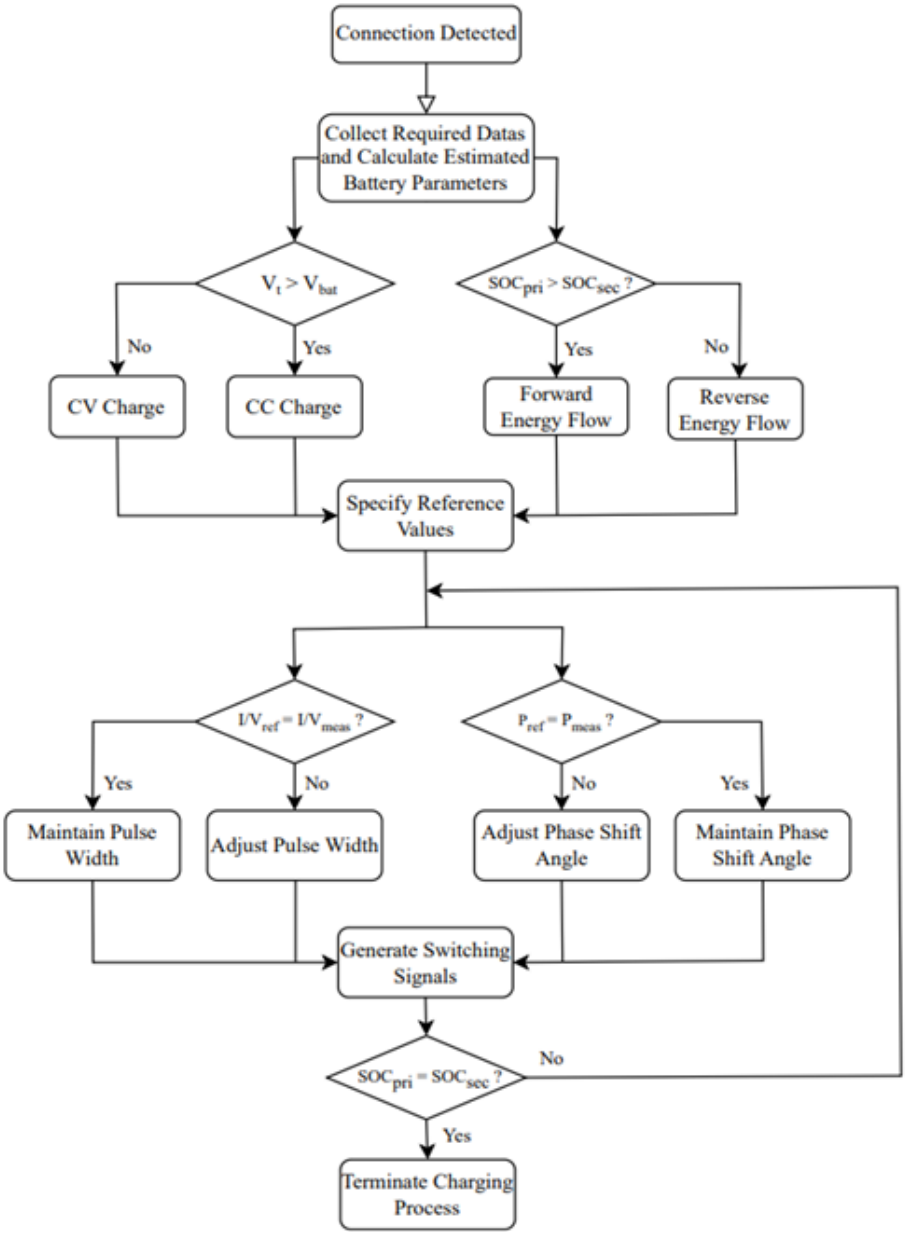

Figure 6. Flowchart of combined modulation strategy

CLLC resonant converter topology in SIMULINK is given by Fig. 7, and for a primary battery of 800V, 50 kWh, and 40% SOC and a secondary battery of 550V, 50 kWh, and 60% SOC, energy transfer will be from the secondary side to the primary side, i.e., reverse transmission. The energy transfer will continue until the batteries' State of Charge (SOC) equals 50% for each battery. Furthermore, if the output side voltage exceeds the input side voltage, the converter will operate in boost mode. Resonant tank gain is 1.4933 at that time, so that, the output voltage can reach up to 1026 V.

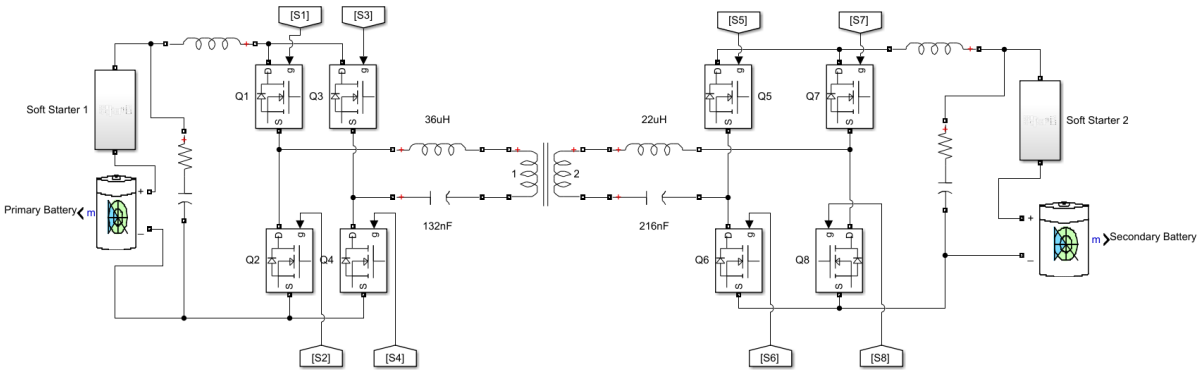

Figure 7. CLLC resonant converter structure in SIMULINK

The remaining regulation could be accomplished by varied modulation techniques; even this paper presents a combined PWM&PSM structure. The flowchart implements a PI controller loop that follows the reference voltage/current to adjust the switching signal's width. Similarly, another loop adjusts the reference power of the converter, which is 11 kW, and then creates a phase shift angle to delay between the two legs of the DAB, thereby meeting the system requirements. Fig. 8 reveals switching signals at steady state condition. Currently, duty ratio is around 58.45% and phase shift angle is around 113.7 degrees. Since the converter operates in reverse mode, these signals switching the switches Q5 and Q7, respectively.

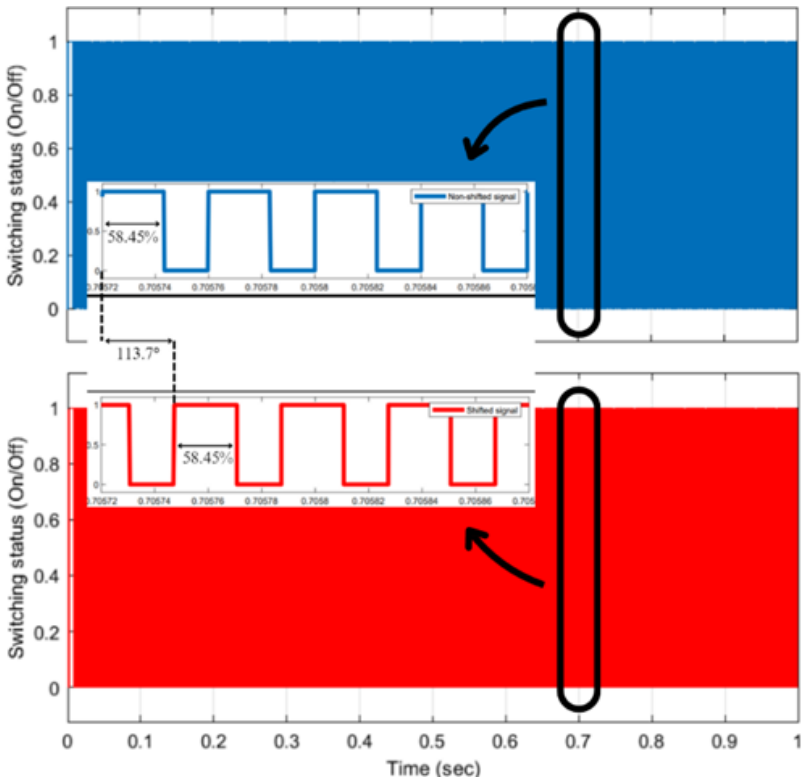

Figure 8. Steady state switching signals

The combined modulation provided by few steps. As could be observed on Fig. 9, first, switching period calculation with 25 kHz of switching frequency, which equals to 40 μs, is done then, a sawtooth reference creation for non-shifted switching pulse, phase shift angle implementation as time delay, a sawtooth reference creation for shifted switching pulse,

multiplication of duty cycle with switching period and lastly comparison with related sawtooth samples is performing in an order.

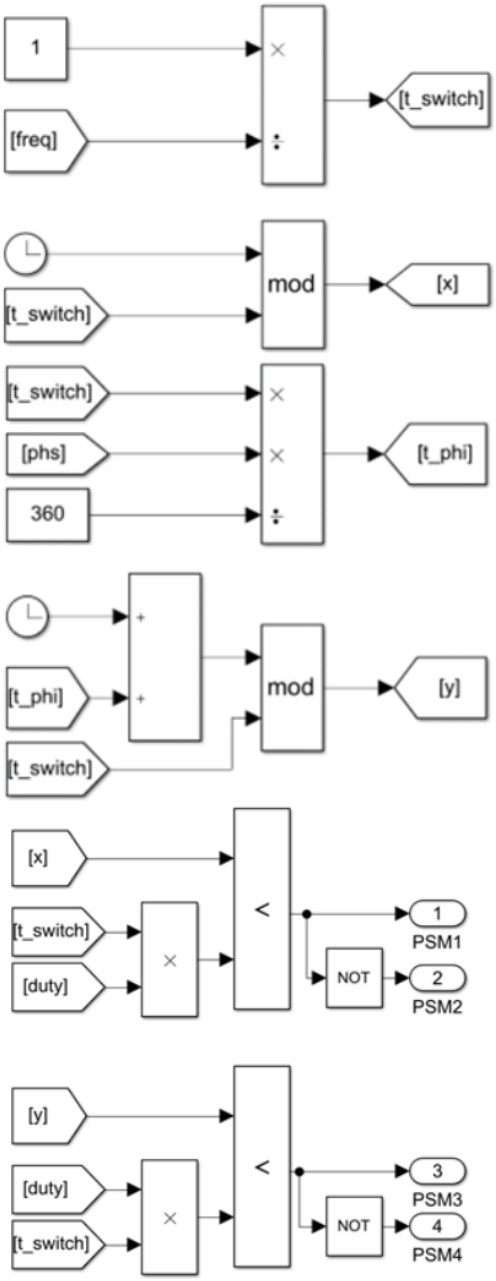

Figure 9. Pulse generation procedure

As a result, the system reaches smoother voltage and current signals at the charge terminal, whilst keeping its efficiency. The lower ripple and lower resonant effect could be observed in Fig. 10 and Fig. 11, respectively.

To affirm the stability of modulation, an instant replacement of batteries on both sides was performed. For all the batteries with 50 kWh capacity, a nominal 800 V and 550 V batteries are connected to primary and secondary side terminals of the converter at the beginning, respectively, then, at 0.5 seconds, a 750 V and a 700 V battery substitute the ones already connected to the terminals.

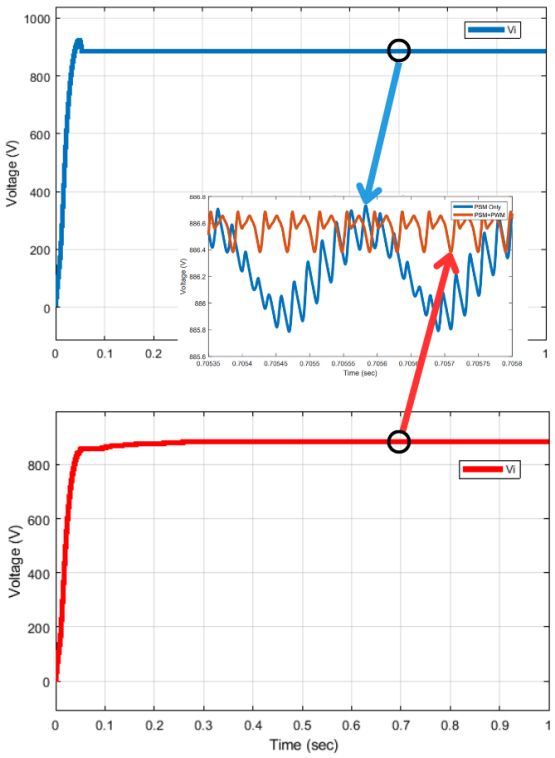

Figure 10. Steady state output voltage waveform with PSM only and PSM&PWM combined modulation technique

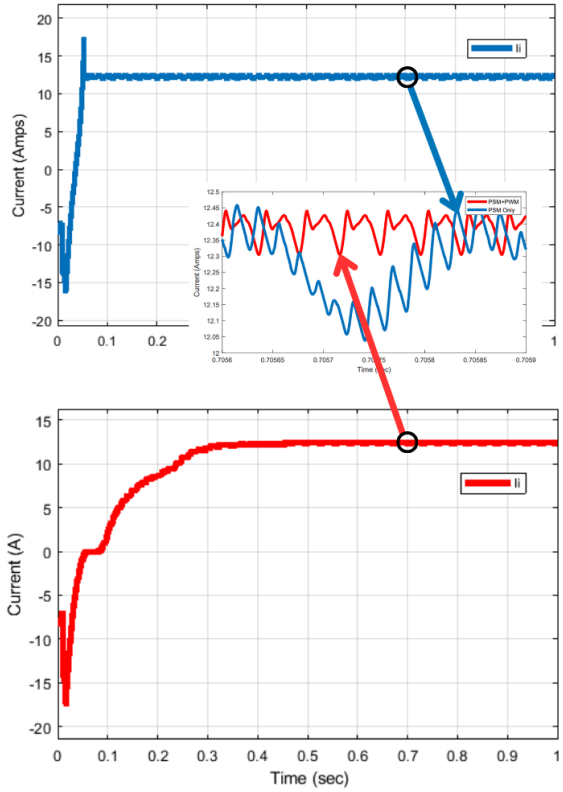

Figure 11. Steady state output current waveform with PSM only and PSM&PWM combined modulation technique

For this transient response interval, duty cycle and phase shift angle are readjusting by their control loops, which Fig. 12, and Fig. 13 show both, from the beginning to the end.

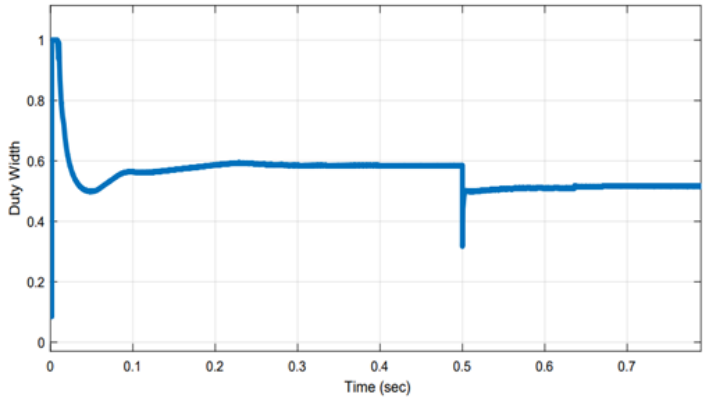

Figure 12. Pulse width during two transient and steady state time intervals (Primary battery: 800V to 750V and Secondary battery: 550V to 700V)

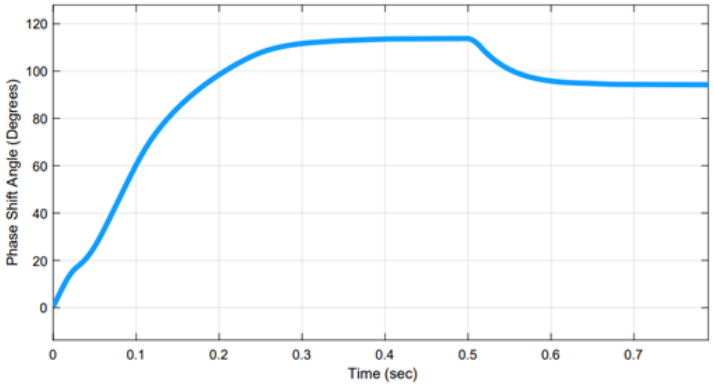

Figure 13. Phase shift angle during two transient and steady state intervals (Primary battery: 800V to 750V and Secondary battery: 550V to 700V)

Also, all the buck, boost, or unity operations in both forward and reverse mode is tested by changing the batteries at both sides of the converter simultaneously. As presented for reverse buck operation, next, there are many test conditions, where a few listed in Table 2.

Table 2. Possible response scenarios test conditions.

Primary battery	**Secondary battery**	**Energy Flow**
800V → 750V	550V	Reverse
700V → 800V	800V	Reverse
750V	800V → 550V	Forward
750V	750V → 700V	Forward
800V → 750V	550V →700V	Forward

Before the break point, when t at around 0.4 to 0.5 seconds, and after the system becomes steady state condition. Later than break, when t at around 0.7 to the end, system reaches steady state

condition second time for two battery combinations. The variation on the output voltage and current waveform is given in Fig. 14 and Fig. 15, respectively.

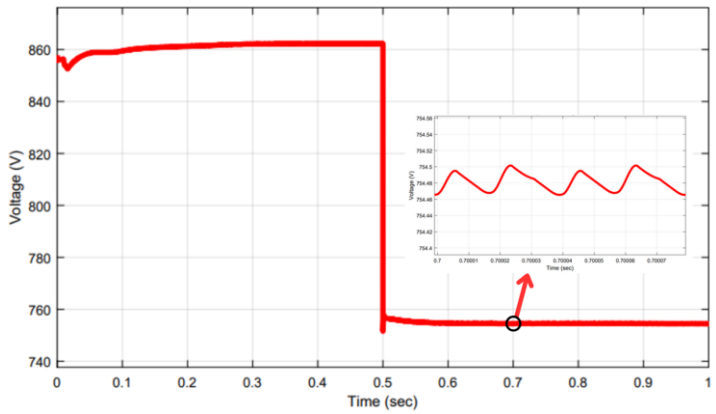

Figure 14. Charging side voltage variation when batteries on both sides are replaced

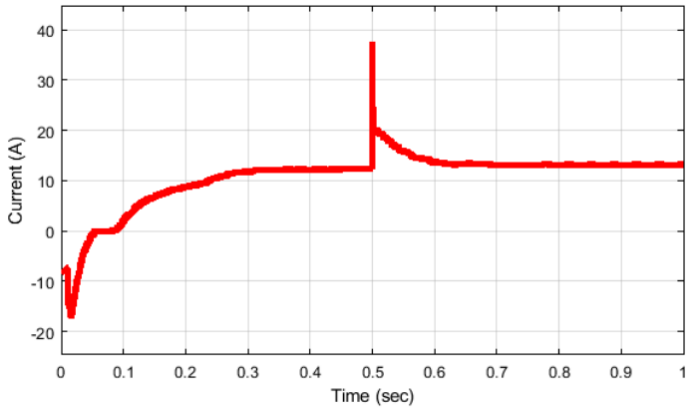

Figure 15. Charging side current variation when batteries on both sides are replaced

The system can handle with instant charge power variation. At t = 0.4 seconds, the converter starts to operate in half power and then at t = 0.7 seconds, becomes full power of operation again. The following figures show the voltage and current waveforms of charging side of the converter and power percentage with respect to converter maximum power. As observed in figures 16, 17 and 18, the system can handle instant power decrement/increment, then continues its operation.

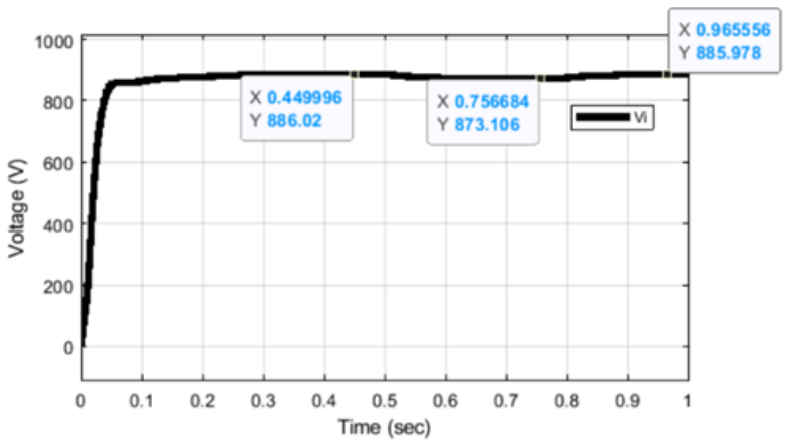

Figure 16. Charge voltage variation when full-load/half-load test is in progress

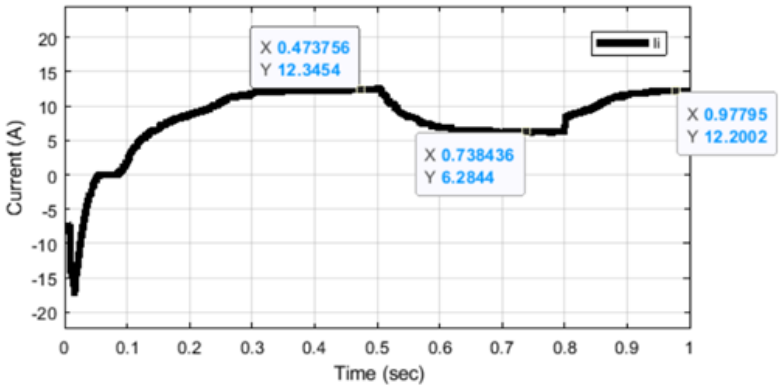

Figure 17. Charge current variation when full-load/half-load test is in progress

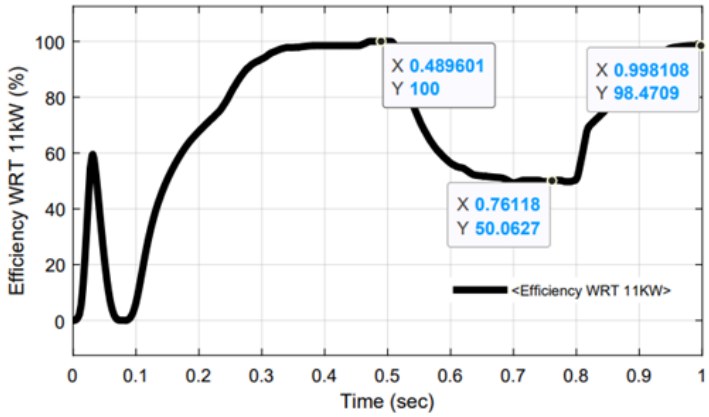

Figure 18. Converter efficiency percentage when full-load/half-load test is in progress

Scenarios are simulated one by one, similarly, and related figures, figure 19, 20 and 21, show the results. Variations on duty ratio, phase shift angle, output voltage and currents appended respectively representing second, third and fourth scenarios according to Table 2.

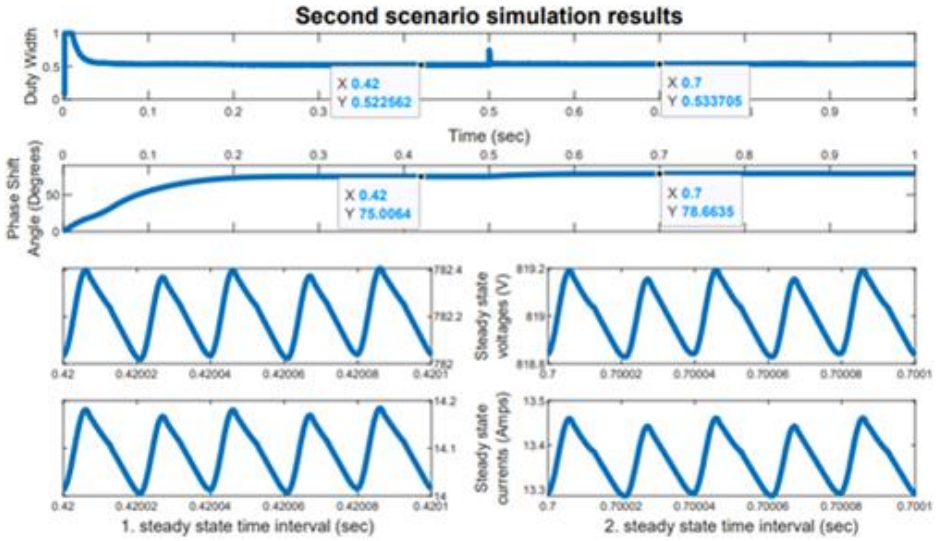

Figure 19. Simulation waveform results for scenario two (Primary battery: 700V to 800V and Secondary battery: 800V)

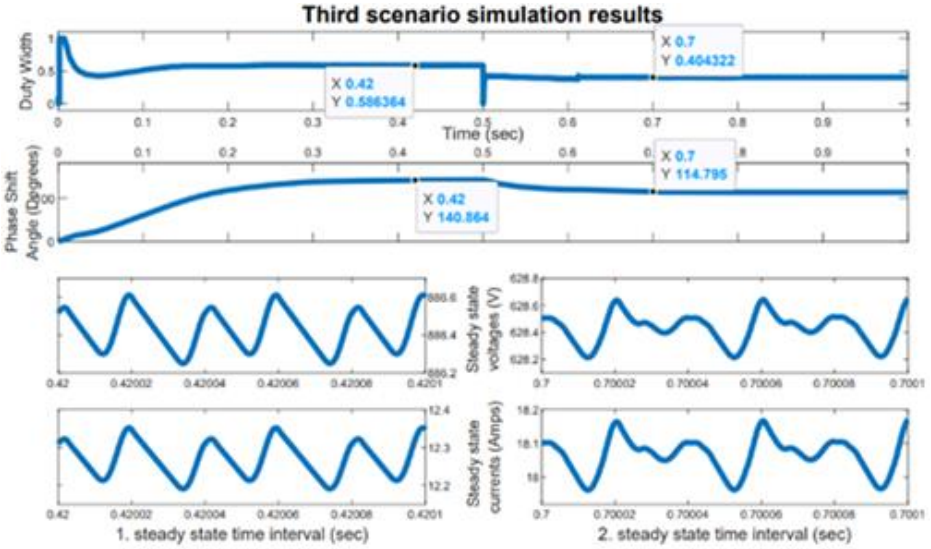

Figure 20. Simulation waveform results for scenario three (Primary battery: 750V and Secondary battery: 800V to 550V)

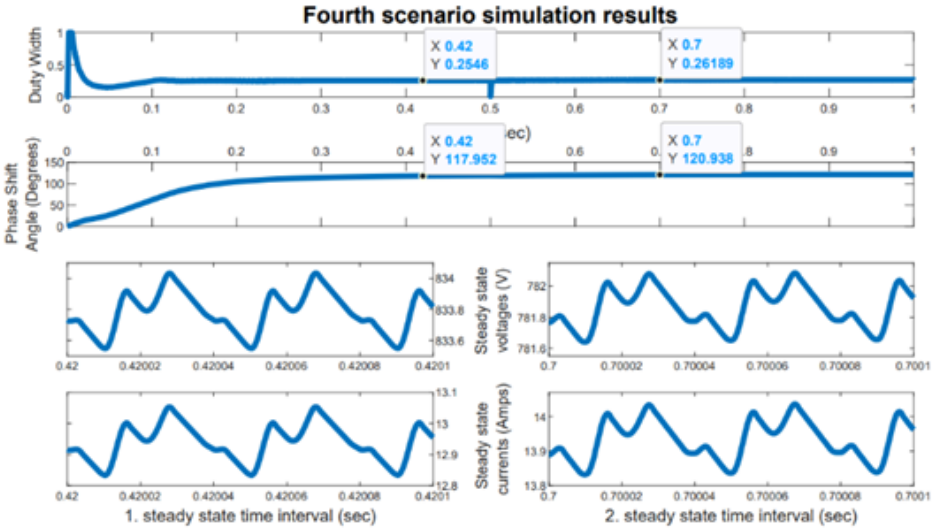

Figure 21. Simulation waveform results for scenario four (Primary battery: 750V and Secondary battery: 750V to 700V)

As evaluated, presented and simulated in sections, a new combined modulation strategy is proved to operate to control bi-directional CLLC resonant converter. Apart from common hybrid modulation techniques studied in [18, 20-25, 30], the PWM&PSM combined modulation is validated to operate with simultaneous parameter variation as could be observed in figures 10, 11, 19, 20 and 21.

5. Conclusion

In this study, a proposed combined modulation strategy integrating PSM and PWM is implemented using the MATLAB/Simulink program. The focus is directed towards its application on a bi-directional CLLC DAB converter, aiming to assess its efficacy in achieving the desired output reference, particularly in comparison with employing a single PSM and PWM control techniques. While numerous hybrid modulation strategies are documented in existing literature, they typically involve toggling between different modulation types. In

contrast, the proposed combined method directly influences both the pulse width and the phase shift angle between the legs of the DAB converter. As explained in preceding sections, the introduced modulation system effectively manages to attain the reference values. Furthermore, it exhibits capabilities in reducing output ripple, mitigating modulation effects, and closely approaching the desired charge power target of 11 kW. The utilization of this combined modulation technique presents a viable alternative to conventional single-switching modulations, showcasing promising prospects for enhancing the performance of DC-DC converters. The study further may provide a printed prototype, be tested for EMI/EMC compability, and finally be produced as a final product.

References

[1] Josevski, M., Korompili, A., Monti, A., "Modelling and Voltage Control of Bidirectional Resonant DC/DC Converter for Application in Marine Power Systems", IFAC, Aachen (2020).

[2] Liu, Y., Du, G., Wang, X., Lei, Y., "Analysis and Design of High-Efficiency Bidirectional GaN-Based CLLC Resonant Converter", Energies (2019).

[3] Sun, L., Ma, Y., Wang, J., Han, J., Suo, X., Li, X., "Analysis and design of assymmetric CLLC resonant DC- DC converter", International Transactions Energy Systems (2020).

[4] Sun, K., Gao, Y., Chen, H., "Bi-Directional High- Conversion-Ratio CLLC Resonant Converter with a New Synchronous Rectification Scheme for Low Conduction Loss", IEEE Journal of Industry Applications (2020) : 512-522.

[5] Lui, C., Wang, J., Colombage, K., Gould, C., Sen, B., "A CLLC Resonant Converter Based Bidirectional EV Charger with Maximum Efficiency Tracking", 8th IET International Conference on Power Electronics, Machines and Drives (PEMD 2016) Glasgow, UK (2016).

[6] Jung, J.H., Kim, H.S., Ryu, M.H., Baek, J.W., "Design Methodology of Bidirectional CLLC Resonant Converter for High-Frequency Isolation of DC Distribution Systems", IEEE Transactions on Power Electronics (2013).

[7] Lin, F., Zhang, X., Li, X., "Design Methodology for Symmetric CLLC Resonant DC Transformer Considering Voltage Conversion Ratio, System Ability and Efficiency", IEEE Transactions on Power Electronics (2021) : 10157-10170.

[8] Wei, Y., Luo, Q., Mantooth, H.A., "LLC and CLLC Resonant Converters Based DC Transformer (DCXs): Characteristics, Issues and Solutions", CPSS Transactions on Power Electronics and Applications, 6(4) (2021) : 332-348.

[9] Zhao, B., Zhang, X. and Huang, J., "Design of CLLC Resonant Converters for the Hybrid AC/DC Microgrid Applications", IEEE International Power Electronics and Application Conference and Exposition (PEAC) Shenzhen, China (2018).

[10] Zahid, Z.U., Dalala, Z.M., Chen, R., Chen, B., Lai, J.S., "Design of Bidirectional DC–DC Resonant Converter for Vehicle-to-Grid (V2G) Applications", IEEE Transactions on Transportation Electrification 1(3) (2015) : 232-244.

[11] Dhakar, A.K., Soni, A., Saini V., Chandel, S., "Design of Bi-directional CLLC Resonant Converter with Planar Transformer and Synchronous Rectification for Energy Storage

Systems", IEEE International Conference on Power Electronics, Drives and Energy Systems (PEDES) Jaipur, India, (2020).
[12] Hasnain, A., Paduani, V., Kondrath, N., Zhou, R., Pant, P., Jiao, Q., "Control Structure for Bidirectional Battery Charger Integrating 3-Φ PFC AC/DC and CLLC DC/DC Converters", IEEE International Conference on Power Electronics, Smart Grid and Renewable Energy (PESGRE2020) (2020).
[13] Dhakar, A.K., Soni, A., Bansal, H.O., "Design and Control of a Bi-directional CLLC Resonant Converter For Low voltage Energy Storage Systems", IEEE 17th India Council International Conference (INDICON) (2020).
[14] Koga, Y., Mishima, T., "Analysis and Verification on CLLC Resonant Bidirectional DC-DC Converter Based on Variable Frequency Phase Difference Control Principle", IEEE 18th International Power Electronics and Motion Control Conference (PEMC) Budapest, Hungary (2018).
[15] Zhu, T., Zhuo, F., Zhao, F., Song R., Wang F., Yi, H., "Analysis of Multiple Phase-shift Control for Full-bridge CLLC Resonant Converter Based on Improved Fundamental Harmonic Approximation Method", IEEE 21st Workshop on Control and Modeling for Power Electronics (COMPEL) Aalborg, Denmark (2020).
[16] Yang, D., Zhang, Y., Liu, X., Wang, W., Liu, J., "Overview of CLLC Modulation Strategy", International Power Electronics Conference (2022).
[17] Youssef, M.Z., Jain, P.K., "A Review and Performance Evaluation of Control Techniques in Resonant Converters", The 30th Annual Conference of the IEEE Industrial Electronics Society Busan, Korea (2004).
[18] Liu, X., Huang, J., Li, G., Ma, P., Tong, X., "Hybrid Pulse Frequency and Width Modulation scheme for Three-port Resonant DC/DC Converters", IECON 2020 The 46th Annual Conference of the IEEE Industrial Electronics Society, Singapore (2020).
[19] Zhu, T., Yu, K., Zhuo, F., Wang, F., Zhao, F., Song, R., "A Novel APWM Control Scheme for GaN Based Full-Bridge CLLC Resonant Converter with Improved Light-Load Efficiency", IEEE Applied Power Electronics Conference and Exposition (APEC) New Orleans, LA, USA (2020).
[20] Li, L., Cao, Y., Hou, L., Mao, T., Ning, W., "PFM-PS Hybrid Control Strategy CLLC Resonant Converter Research". 8th Asia Conference on Power and Electrical Engineering (ACPEE) (2023).
[21] Wei, Y., Luo, Q., Montooth, A., "Overview of Modulation Strategies for LLC Resonant Converter", IEEE Transactions on Power Electronics (2020) : 10423- 10443.
[22] Wei, Y., Woldegiorgis, D., Mantooth, A., "Control Strategies Overview for LLC Resonant Converter with Fixed Frequency Operation", IEEE 11th International Symposium on Power Electronics for Distributed Generation Systems (PEDG) Dubrovnik, Croatia (2020).
[23] Xie, M., Bi, K., Ai, J., Fan, Q., "A Hybrid Control Strategy for CLLLC Resonant Converter Based on PS-PFM under Wide Input Voltage", 26th International Conference on Electrical Machines and Systems (ICEMS) (2023).
[24] Qin, M., Zhang, F., Ye, A., Huang, L., Tian, Q., "A Novel Hybrid Modulation Strategy of LLC Resonant Converter with Capacitive Load", IEEE 4th International Electrical and Energy Conference (CIEEC) (2021).

[25] Kececioglu, O.F., Gani, A., Sekkeli, M., “Improved hybrid intelligent controller design for MPPT of stand-alone PV System”, Turkish Journal of Engineering 5(1) (2021) : 20-28.

[26] Zou, S., Lu, J., Mallik, A., Khaligh A., “Bi-Directional CLLC Converter With Synchronous Rectification for Plug-In Electric Vehicles”, IEEE Transactions on Industry Applications 54(2) (2018) : 998-1005.

[27] Duan, C., Bai, H., Guo, W., Nie, Z., “Design of a 2.5-kW 400/12-V High-Efficiency DC/DC Converter Using a Novel Synchronous Rectification Control for Electric Vehicles”, IEEE Transactions on Transportation Electrification 1(1) (2015) : 106-114.

[28] Jinglu, C., Fengrui, Z., Yonghui, D., Xinzheng, W., “Design of Synchronous Rectification DC-DC Converter”, IEEE 5th Advanced Information Technology, Electronic and Automation Control Conference (IAEAC) (2021).

[29] Burdio, J.M., Canales, F., Barbosa, P.M., Lee, F.C., “A Comparison Study of Fixed-Frequency Control Strategies for ZVS DC/DC Series Resonant Converters”, 32nd Annual Power Electronics Specialists Conference Vancouver, BC, Canada (2001).

[30] Fang, Z., Xie, F., Huang, Z., “Hybrid PFM and PWM Modulation Scheme for Series Resonant Bidirectional DC/DC Converter”, 9th International Power Electronics and Motion Control Conference.